ACS APPLIED MATERIALS & INTERFACES

Surfaces, Interfaces, and Applications

Multilayered Nanoplasmonic Arrays for Self-Referenced Biosensing

Justin R. Sperling, Gerard Macias, Steven Neale, and Alasdair W. Clark

ACS Appl. Mater. Interfaces, **Just Accepted Manuscript** • DOI: 10.1021/acsami.8b12604 • Publication Date (Web): 12 Sep 2018

ACS Publications

is published by the American Chemical Society. 1155 Sixteenth Street N.W., Washington, DC 20036

Multilayered Nanoplasmonic Arrays for Self-Referenced Biosensing

*Justin R. Sperling‡, Gerard Macias‡, Steven L. Neale, and Alasdair W. Clark**

Biomedical Engineering Research Division, School of Engineering, University of Glasgow, G128LT, UK

Keywords: plasmonics, biosensor, LSPR, self-referencing, multilayer

ABSTRACT

Nanostructured sensors based on localized surface plasmon resonance (LSPR) offer a number advantages over other optical sensing technologies, making them excellent candidates for miniaturized, label-free chemical and biological detection. Highly sensitive to local refractive index changes, the resonance peaks of the nanosensors shift by different amounts when subject to different biological and chemical environments. Modifications to the nanostructure surface allow for detection of specific molecules and chemicals with shifts so sensitive that the presence of single molecules can be detected. However, this extreme sensitivity has its drawbacks. Resonance shifts also occur due to temperature shifts, light-intensity fluctuations, and other environmental factors. In order to distinguish detection from drift, a secondary sensor region is often required. This often

doubles the size of the device, requires two light sources and detectors (or complex optics), doubles the sample volume required (which may be expensive, or may not be possible if sample quantity is limited), and subjects the reference to potential biofouling. Here, we present a new proof-of-concept multilayered LSPR sensor design that incorporates both a sensing layer and an encapsulated reference layer within the same region. By doing so, we are able to monitor and correct for sensor drift without the need for a secondary reference channel. We demonstrate that suitability of this sensor for sucrose concentration measurements and the detection of biotin-avidin interactions, while also showing that the sensor can self-correct for drift. We believe that this multilayer sensor design holds promise for point-of-care diagnostics.

Introduction

Surface plasmon resonance (SPR) has long been used as a label-free optical biosensing technique. [1] While a powerful tool for sensing, the use of SPR sensors in point-of-care devices is typically hindered by miniaturization problems and complex supporting optics [2-3]. As an alternative, sensors based on localized surface plasmon resonance (LSPR) have been demonstrated to have similar performance to SPR sensors. [4] While SPR relies on the propagation of surface plasmon polaritons on a continuous metal film, LSPR is localized to structures on the nanoscale. Therefore, LSPR allows for the use of more compact optics, does not need precise temperature control, and thus has the potential to be miniaturized beyond the capabilities of SPR sensors. [5] For example, LSPR sensors were demonstrated in the parallel biosensing of 32 independent sensor elements on the same chip. [2]

LSPR sensors have a characteristic spectral response governed by the size, arrangement, shape, and material of nanoparticles that the make up the sensor. Additionally, the interaction of the surface plasmons of the nanoparticles with the local environment (about 100 nm) surrounding them, external light source, and external temperature also affects the response. Binding events are thus typically measured by detecting a shift in the spectral response from the baseline caused by the interaction of the LSPR with captured particles. This highly localized sensing minimizes bulk refractive index (RI) effects [3, 6-7] and has been used for real-time, label-free detection of nanoscale biochemical events such as protein-substrate binding [5-6, 8-9], antibody-antigen binding [2-3, 10], and DNA base pairing. [5, 11-13]

Since LSPR sensing devices are responsive to many different changes on the nanoscale, a major challenge in real-time detection with LSPR sensing devices is determining if a measured shift in response arises from a desired signal or some sort of drift in the baseline. [14] This is especially problematic for devices designed for point of care applications, where a sensor is more likely to be exposed to environments where precise control of external factors—such as intensity fluctuations of the light source for example—is not possible. To account for such drifts, a reference for the sensing device is necessary. The standard method to account for baseline drift from the environment is to use a separate reference flow channel. [15-16] However, this approach neglects the possibility that the events in two separate channels may differ.

To overcome this challenge, a variety of sensor technologies with the capability to self-reference have been explored. Examples include dual-metal SPR sensors, [17-18] modified Mach-Zehnder Interferometer phase sensors, [19-21] porous silicon double layer sensors, [22-23] photochemical sensors, [24] nanohole LSPR sensors, [25] refractometric LSPR sensors, [26] dual-metal suspended colloid LSPR sensors, [27] and polarization-dependent sensors, [14] to name a few.

Here, we present a multilayered LSPR sensor with internal-referencing that self-corrects for baseline drift. Comprised of both an encapsulated and an exposed nanoplasmonic layer, this device exhibits two distinct peaks—a reference peak from the encapsulated layer and an active, sensing peak from the exposed layer. The encapsulated reference layer corrects for drift that could occur during real-time chemical and bio-sensing experiments.

Analysis using the position of each peak allows for the correction of baseline drift. More accurate referencing is achieved because the design of the sensor allows for a single spot within one channel to produce two signals from a single light beam. [17] Additionally, utilizing one channel rather than separate sensing and referencing channels allows for a more compact design and eliminates the need to inject potentially expensive samples into a non-capturing parallel reference channel. [17]

Our design offers advantages over other self-referencing technologies in that the reference of the device does not require highly accurate spatial control over the different surface modifications of the sensing device [17-18] and is not subject to fouling because the reference layer is isolated from the sensing region. [17-18, 22-26] Additionally, our device self-corrects rather than just recognizing "unreliable data," [24] can be regenerated and thus reused in multiple detection events rather than being consumed during detection, [27] and doesn't require multiple detectors [26] or a beam-splitter. [14]

Experimental Section

Device Fabrication: Devices were fabricated using electron-beam lithography, inductively coupled plasmon chemical vapor deposition (ICP-CVD), and metal-evaporation. For both the reference and sensing nano-antenna layers, a resist bi-layer of 4% poly(methyl methacrylate) resist

(PMMA) 2010 and 2.5% PMMA 2041 (total thickness 150 nm) was patterned using a Vistec VB6 Ultra High Resolution Extra Wide Field electron beam lithography tool. Following development of the pattern, a 2/50 nm Ti/Au layer was evaporated onto the sample using a Plassys MEB 400S/550S electron-beam evaporation tool. The silicon nitride layer was deposited using an Oxford Instruments System 100 ICP 180 PECVD nitride deposition tool at room temperature. A J.A. Woollam Mark II Variable Angle Spectroscopic Ellipsometer was used to determine the thickness and dielectric (n,k) values of the nitride. To planarize the nitride layer, hydrogen silsesquioxane (HSQ, Fox 16) was spun on and then cross-linked using the electron-beam lithography tool. The final sensing nano-antenna layer was then fabricated on top of the HSQ layer, following the same procedure as the fabrication steps of the reference layer.

Experimental Setup: A polydimethylsiloxane (PDMS) microfluidic channel was placed on top of the device and a positive crankcase ventilation (PVC) value was used to allow for injections of the molecules for detection without disrupting flow. The flow rate from the microfluidic pump was set to 100 $\mu L \cdot min^{-1}$. A custom-built microspectrophotometer was used to measure the real-time transmission spectra (0.5 nm resolution). Light from a visible to near-infrared (VIS-NIR) light source (tungsten-halogen 400 to 1200 nm wavelength) was used to probe the sensor. A 10x objective was used to couple the transmitted light into an optical-fibre attached to a StellarNet Microspectrophotometer (StellarNet Blue Wave). Sample rates of 7.5 seconds for the refractive index calibration experiment and 3.5 seconds for the biotin-avidin experiment were used to capture a 30-measure-averaged transmission response of the device.

Peak-Analysis: MatLab and Origin were used to analyze of the transmission spectra for each series of the real-time measurements. The transmission spectrum was smoothed (20 points, mean-average smoothing) and interpolate (from 0.5 nm to 0.01 nm). The peak position value of the two

minima peaks and full-width half-max (FWHM) values were determined. The corrected position response (CPR) was calculated by subtracting the position of the sensing peak from the reference peak.

Sensor Calibration: For the calibration experiments, water was flowed over the device using the experimental setup, and varying concentrations of sucrose (Sigma Aldrich) from 0.5% to 50% (w/w) dissolved in water were injected into the system. The refractive index of the surrounding medium was, thus, altered from 1.333 to 1.4201. [28]

Device functionalization: The sensor was immersed in a 10 mM ethanolic solution of 11-mercaptoundecanoic acid (MUA, Sigma Aldrich) overnight, rinsed three times with ethanol, dried under a stream of nitrogen, and assembled into the microfluidic system where a constant flow rate of 100 $\mu L \cdot min^{-1}$ was maintained throughout the experiments. The channel was flushed with water for 20 min prior to the injection of 500 µL of 200 mM (1-Ethyl-3-(3-dimethylaminopropyl)-carbodiimide) (EDC, Sigma Aldrich) in MES buffer at pH 5.5 and rinsed with de-ionized (DI) water for 15 min. 500 µL of 500 $\mu g \cdot mL^{-1}$ biotin hydrazide (Sigma Aldrich) in DI water was then injected, followed by a DI water rinse for a further 15 min. Finally, unreacted sites were blocked with 500 µL of 1 M ethanolamine (Sigma Aldrich) in DI water and rinsed with DI water for 15 min.

Biological sensing: 0.1% Tween-20 in phosphate buffer saline (PBS) was used as the flowing solution throughout the experiments. Prior to the biological sensing, the device was stabilized by flowing the PBS solution at 100 $\mu L \cdot min^{-1}$ for 30 min. Throughout the experiments, the flow rate was kept constant at 100 $\mu L \cdot min^{-1}$ and at least 10 min of baseline were acquired before the biomolecule injection. Sensor regeneration was achieved by injecting 500 µL of 20 mM sodium

hydroxide in DI water. As a non-specific control, 500 μL of 100 μg·mL^{-1} bovine serum albumin was injected. Finally, 0.1, 1, 100 and 500 μg·mL^{-1} of avidin in 0.1% Tween-20 PBS was injected at a constant volume of 500 μL in order to test the specificity and dose-dependency of our device.

Results/Discussion

The multilayered substrate design (**Figure 1**) consists of two 100 nm x 100 nm x 50 nm (L x W x H) gold nanoarrays—an encapsulated reference array (Figure 1a) and exposed sensing array (Figure 1d). Nano-square shapes were chosen for this proof-of-concept device because (1) the design allows for easy, repeatable fabrication, (2) the symmetrical shape is not subject to a polarization-dependent response, and (3) the shape maximizes the surface area of coverage for a given periodicity (and thus maximizing the plasmonic signal). A periodicity of 300 nm was chosen because this period provides a significant enough distance between particles to make plasmon coupling negligible [29] but close enough to provide good coverage of structures for a strong plasmonic signal (>90% transmission-attenuation).

By encapsulating the reference array in silicon nitride (Figure 1b), its LSPR is isolated from the environment of the exposed sensing array. [6] This design removes the reference from the detection events in the sensing layer but allows for simultaneous detection of changes in the external environment of the testing site. The silicon nitride layer, however, conforms to the surface it is deposited on (as indicated in both the SEM and AFM of Figure 1b) and thus is not suitable as a base for the fabrication of the sensing layer. Planarization was achieved by depositing HSQ on top of the silicon nitride (as shown by comparing the SEM and AFM images in Figure 1b and Figure 1c).

As the purpose of this design is to evaluate the viability of the multilayer design for self-referencing, neither the structure geometry of the nanostructures nor the array periodicity was optimized to produce the most sensitive device. Instead, examination of the insulating layers was conducted (see Supporting Information) to determine (1) the minimum value of silicon nitride thickness necessary to keep the reference layer insulated from the above environment and (2) the minimum value of HSQ needed to planarize the nitride capped layer so that fabrication of the second plasmonic array could occur. Silicon nitride above 80 nm isolates nanostructures of a variety of dimensions (plateau region in **Figure S2b(ii)**), and a separation between the two plasmonic layers greater than 100 nm exhibits minimal coupling (**Figure S3**). The 100 nm x 100 nm x 50 nm (L x W x H) structure was confirmed to provide the largest signal attenuation for all thicknesses of nitride deposition and therefore would suffice as good dimensions for a proof-of-concept design. HSQ with a thickness of 200 nm was found to planarize the surface (**Figure S5**). To ensure that the reference layer of the device used for experimentation was isolated and the second array layer was fabricated on a planar surface, 100 nm of silicon nitride (86.59 ± 0.042 nm as measured by ellipsometry) and 320 nm of HSQ were used. These values were well into (1) the plateau region of the silicon nitride curves and (2) beyond that found necessary to planarize the surface with HSQ. The total thickness of the insulating layer was also well beyond the minimum separation distance necessary to minimize coupling between two vertically displaced plasmonic nanostructure arrays.

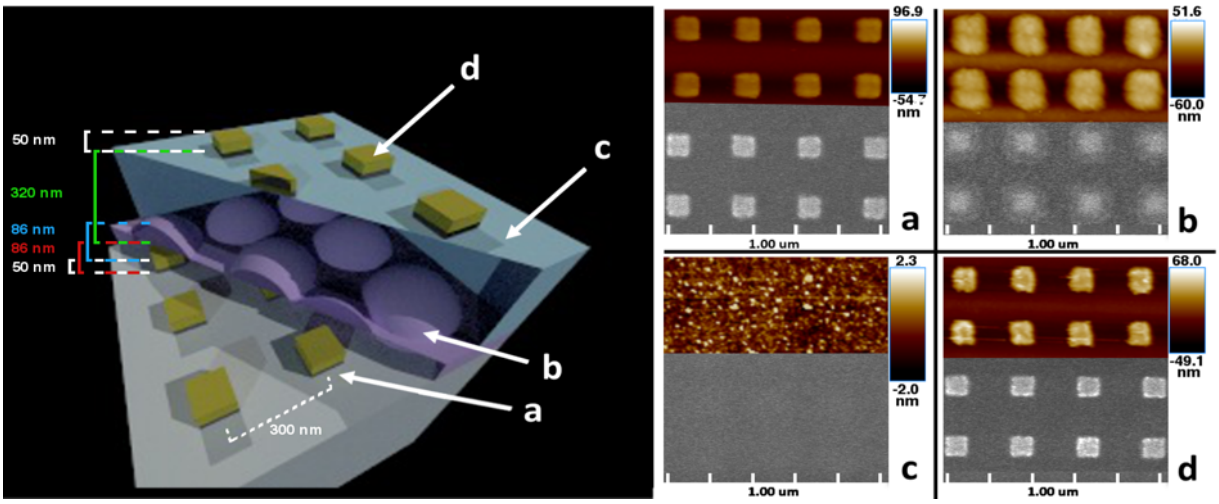

Figure 1: Schematic and SEM/AFM images of a multilayered sensing device. (left) Schematic showing the multilayered device. **(a)** A gold nanostructure LSPR reference layer encapsulated in **(b)** layer-conforming silicon nitride with **(c)** an HSQ planarization layer, and **(d)** a gold nanostructure LSPR sensing plasmonic layer. The nanostructures are 100 x 100 x 50 nm (L x W x H). **(right)** AFM (top) and SEM (bottom) images of each of the device layers (a-d) taken at the time of deposition. The AFM images confirm that the HSQ layer planarized the form-following surface of the nitride layer.

The double plasmonic layer design of the device results in two peaks in the transmission response, denoted as P_1 and P_2 in **Figure 2**, corresponding to the responses of the sensing peak and reference peak, respectively. To correct for drift in peak position, the corrected peak-response (CPR) was calculated by subtracting the position of the sensing peak from that of the reference peak:

$$CPR\ [nm] = P_2 - P_1 \quad (1)$$

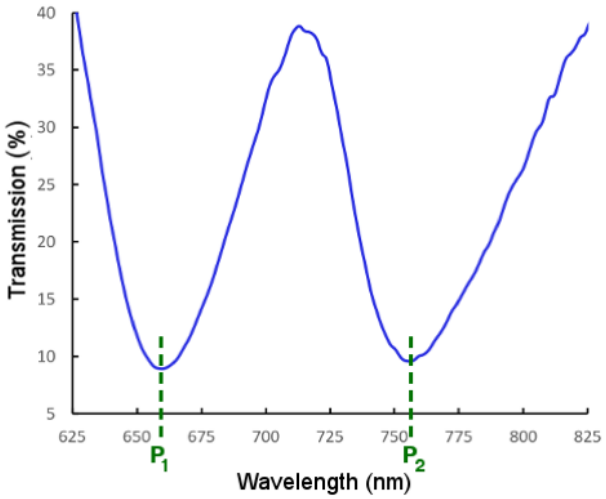

Figure 2: Corrected Peak Response (CPR). CPR is defined as the difference between the sensing peak (P_1) and encapsulated reference peak (P_2).

To measure the spectral response of the sensor, a custom-made microspectrophotometer was used to measure the transmission response caused by fluid flow through a polydimethylsiloxane (PDMS) microfluidic channel placed on top of the device. The stability of the reference peak is demonstrated in **Figure 3a** and **Figure 3b**. When the refractive index of surrounding the sensor is changed from that of water (RI=1.333) to that of 20% (w/w) sucrose solution (RI=1.3639), a clear shift in P_1 occurs while P_2 remains constant (Figure 3a). Figure 3b expands upon this, showing a contour plot of the transmission of the sensor with varying refractive indexes of 1.333, 1.3405, 1.3478, 1.3555, 1.3639, and 1.4201. The reference peak (right-most dashed line) does not exhibit a shift in response with varying refractive index while the sensing peak (left-most dashed line) does. This indicates that the encapsulated peak is a viable reference, independent from the refractive index changes of the sensing region. The reference peak can, therefore, be used to correct both the position and transmission of the sensing layer.

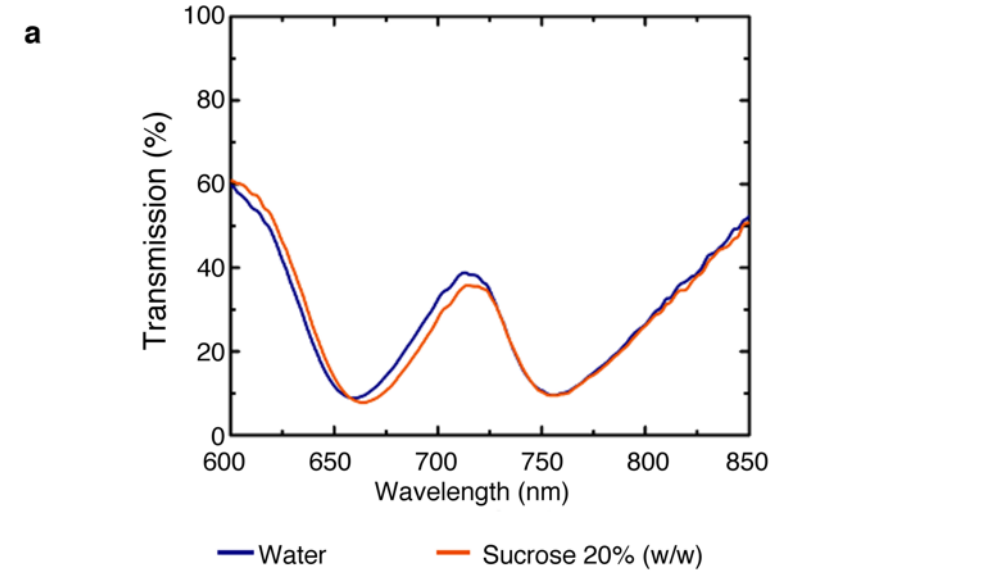
a
Transmission (%)
Wavelength (nm)
Water
Sucrose 20% (w/w)

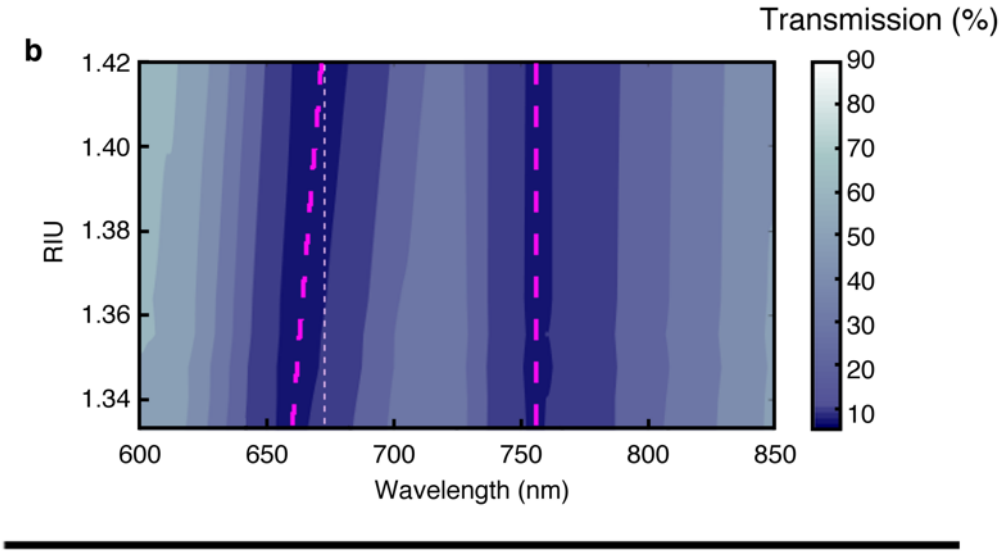
b
Transmission (%)
RIU
Wavelength (nm)

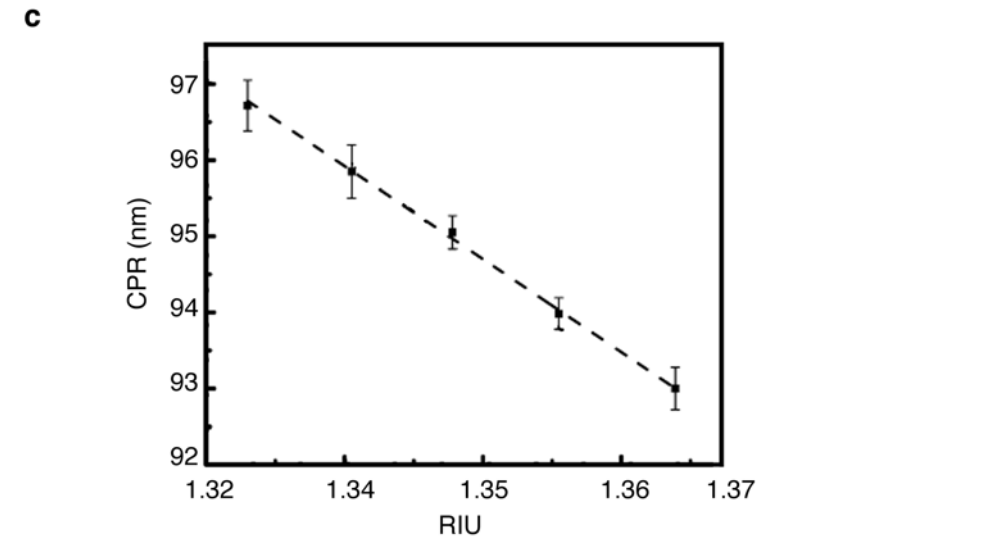
c
CPR (nm)
RIU

Figure 3: Experimental data from multilayered device. (a) Transmission plot of the device in response to water (RIU = 1.333) and 20% sucrose (w/w) (RIU = 1.3639). **(b)** Contour plot of the transmission of multilayered sensor in 0%, 5%, 10%, 15%, 20%, and 50% (w/w) sucrose solutions. Significantly, the encapsulated reference peak (right-most dashed line) does not exhibit a shift in response with varying refractive index while the uncapped sensing peak (left-most dashed line) does. **(c)** Experimental results of the corrected position-response (CPR) to changes in the refractive index. The experimental CPR has a sensitivity of 122 ± 3 nm·RIU^{-1}. The CPR curve is best described with a linear fit because it has an adjusted R^2 value well above 99%.

The sensitivity of the sensor was determined by taking the slope of the CPR-Refractive Index curve (Figure 3c). The CPR sensitivity of 122 ± 3 nm·RIU^{-1} and Figure of Merit (FoM) [30] of 1.3 makes it close to the sensitivity of silver nanocubes,[31] but overall, at the lower sensitivity range of other LSPR sensing devices, which range from 90 nm·RIU^{-1} to 1000 nm·RIU^{-1} and FoM of 0.8 to 5.4. [3, 5-7] As a proof-of-concept, this design shows potential as a new means to self-refence. It is postulated that utilizing this multilayer design with plasmonic structures known to be more sensitive, such as a dimer design, [26] will improve the sensitivity.

To further demonstrate the stability, real-time measurements of induced refractive index changes were measured. **Figure 4a** shows the real-time position response of the sensing peak (black), reference peak (red), and self-corrected response (blue) of the sensor to injections of sucrose solutions in water (green dashed lines) with varying refractive indexes. The injections (in percent weight by weight) for the runs were (i) 0%, 5%, 10%, 15%, 20%, and 50%, (ii) 0%, 0.5%, 1.0%, 2.5%, 5%, 10%, 15%, and 20%, and (iii) 0%, 5%, 10%, 15%, and 20%. For each run, the device was left to stabilize at baseline and injections of sucrose were only started after 10 minutes of a stabilized response was determined. During the first 20 minutes, the device is stabilizing at

baseline. The measurements in Figure 4a(ii) and Figure 4a(iii) were taken in succession of the previous set of measurements. In the first 10 minutes of the measurements of these two runs, the sensor was still returning to baseline from the last injection of sucrose of the previous run. **Figure 4b** shows the shift in the (i) sensing layer, (ii) reference layer, and (iii) calculated CPR from the baseline measurements for the five injections shown in Figure 4a(i). The sensing peak position and CPR both show a step-wise change in response when higher concentrations of sucrose-water are injected in the system while the reference does not. Since the measurements of the second run (Figure 4a(ii)) have the most fluctuation, this run was used to determine the noise, limit of detection, and limit of quantification of the sensor. Using the full ten minutes prior to the first injection of run 2 as the baseline, the standard deviation of the baseline (noise), limit of detection (2x noise), and limit of quantification (3x noise) were determined from the CPR. [32] The sensitivity for CPR was then used to calculate the corresponding change in refractive index. The limit of detection and quantification for the sensor by CPR are changes of 1.52×10^{-3} RIU and 2.28×10^{-3} RIU respectively (see **Table 1**). While these values are also on the lower end of other published LSPR sensor devices, [6-7, 33] we have successfully demonstrated a new design for self-referencing devices that can now be modified with much more sensitive nanostructure arrays. What is important to note is the reduction of noise and correction of drift present in the real-time measurements of CPR compared to the responses of the sensing and reference layers, alone, and other self-correcting devices.

Table 1: Noise-level, limit of detection, and limit of quantification for CPR and the corresponding RI values

	Corrected Position Response	
	ΔCPR	ΔRIU (CPR)
Noise-Level	9.28×10^{-2}	7.59×10^{-4}
Limit of Detection	1.86×10^{-2}	1.52×10^{-3}
Limit of Quantification	2.78×10^{-2}	2.28×10^{-3}

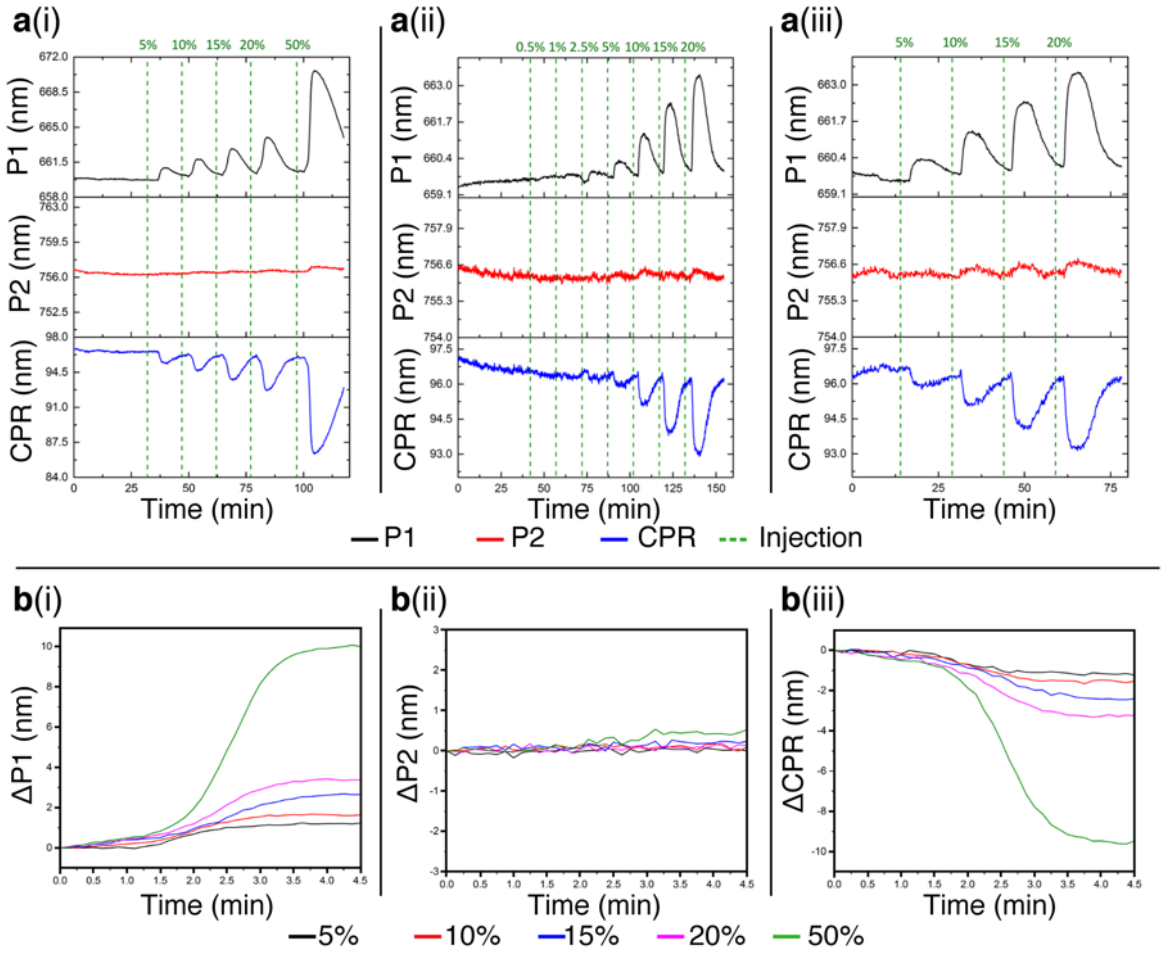

Figure 4: Real-time response of sensor to changes in refractive index. (a) The real-time response of the sensing layer P1 (black), reference layer P2 (red), and calculated CPR (blue) to varying refractive index changes using sucrose solutions (w/w in water) of **(i)** 0%, 5%, 10%, 15%, 20%, and 50%; **(ii)** 0%, 0.5%, 1.0%, 2.5%, 5%, 10%, 15%, and 20%; and **(iii)** 0%, 5%, 10%, 15%, and 20%. The dotted green lines indicated the time at which sucrose was injected into the system. For each run, during the first 10 minutes, the device is stabilizing at baseline. The measurements in (a)ii and (a)iii were taken in succession of the previous set of measurements. In the first ten minutes of the measurement, the sensor was returning to baseline from the sucrose solution of the previous run. **(b)** The shift in peak for **(i)** the sensing layer, **(ii)** the reference layer, and **(iii)** calculated CPR for the five injections from (a)i.

To demonstrate the applicability of the self-correcting device for biosensing applications, we performed a biochemical binding assay. For this purpose, we chose the well-known biotin-avidin interaction as a model. Prior to the real-time measurements, the nanoplasmonic device was functionalized with 11-mercaptoundecanoic acid (MUA). [33-34] This treatment provided a self-assembled monolayer (SAM) with carboxylic acid moieties that were further used to covalently attach biotin-hydrazide via ethylcarbodiimide cross linking. [34] Unreacted sites on the nanostructures were blocked with ethanolamine [33], and Tween-20 was added to the phosphate buffer saline solution used during the biosensing experiment to prevent avidin from binding to unblocked regions of the glass base of the device.

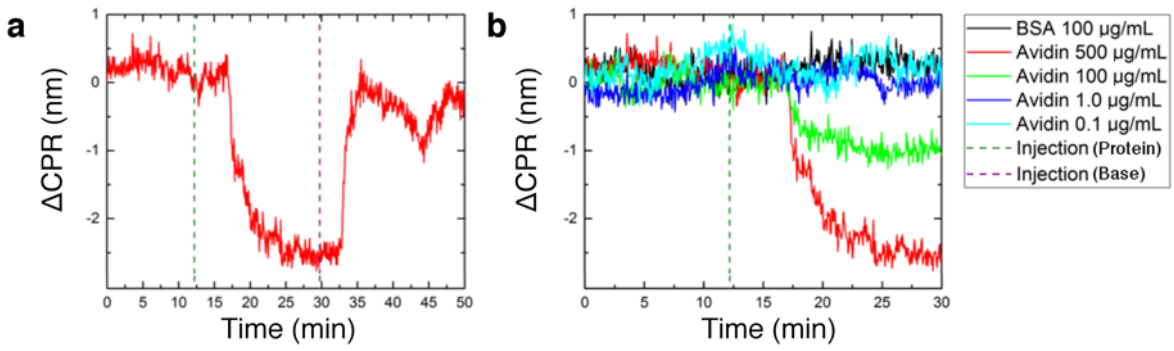

Figure 5: Real-time biosensing of the Biotin-Avidin interaction. (a) The real-time change of CPR to the specific binding and pH-mediated release of 500 $\mu g \cdot mL^{-1}$ avidin to biotin attached to the gold nanostructures on the surface of the sensing region of the device. The dotted green line denotes avidin injection. The dotted purple line denotes when 20 mM NaOH was injected to mediate the release of the protein from the surface. The fluctuation after NaOH injection is present because of the change of the refractive index of solutions flowing through the device. Prior to injecting any other concentrations of protein into the device, a long flush with PBS was done to return the signal to baseline. **(b)** The real-time change of CPR to the non-specific interaction of BSA (100 $\mu g \cdot mL^{-1}$) and the specific binding of avidin (0.1, 1, 100, and 500 $\mu g \cdot mL^{-1}$) with biotin. The dotted line in plot denotes the time at which the protein was injected into the system.

Figure 5a shows the change in CPR to an injection of 500 $\mu g \cdot mL^{-1}$ avidin (green dotted line). To regenerate the surface after protein binding, 20 mM NaOH was injected into the device (purple dotted line). In order to verify the suitability of the sensor in providing a dose-dependent response, tree additional concentrations of avidin (0.1, 1, and 100 $\mu g \cdot mL^{-1}$) were injected. Additionally, the specificity of the sensor was tested by injecting bovine serum albumin (BSA) at a concentration of 100 $\mu g \cdot mL^{-1}$. **Figure 5b** shows the CPR response to BSA and all four concentrations of avidin.

CPR is able to detect avidin in a dose-dependent manner. We also observed the injection of 100 $\mu g \cdot mL^{-1}$ of BSA did not produce a significant shift in the response of our sensor, thus demonstrating the specificity to avidin. However, the concentrations where a significant shift could be observed were 100 and 500 $\mu g \cdot mL^{-1}$. The sensitivity may be improved by investigating different antenna geometries.

Conclusion

In summary, we presented a proof-of-concept multilayered LSPR device with an encapsulated reference region that exhibits drift self-correction. We successfully demonstrate the use of the device as a biosensor to detect selectively and in a dose-dependent manner the biotin-avidin interaction. We believe that combining the concept of an encapsulated referencing layer with different LSPR structures may improve the sensitivity. The inclusion of both the reference and sensing regions within the same physical space allows for a more compact design, eliminates the need to inject samples that are potentially expensive or of limited quantity into a non-capturing parallel reference channel, and allows for the use of a single detector rather than multiple detectors. This is especially of interest for point-of-care diagnostic devices because the self-referencing design accounts for limitations in resources and sample quantity, operates in transmission-mode (standard UV-Vis instrumentation at point of care is generally carried out in this mode), [55] and can be incorporated into multiplexed microfluidic systems.

ASSOCIATED CONTENT

Supporting Information.

Simulations to determine minimum nitride thickness and minimum vertical distance between nanostructure array layers, experimental determination of minimum HSQ layer thickness, full device simulations, and measurements of refractive index values of the nitride layer. All supporting information is available here <link to supplemental section> or from the author.

AUTHOR INFORMATION

Corresponding Author

*Email: alasdair.clark@glasgow.ac.uk

Author Contributions

All authors conceived and designed the experiments. All authors contributed to the writing and editing of the manuscript. J.R.S. and G.M. simulated, designed, and fabricated the devices, performed the experiments, and evaluated the data. J.R.S. and G.M. contributed equally to the work. A.W.C. and S.L.N. coordinated and supervised the work. All authors have given approval to the final version of the manuscript.

‡These authors contributed equally.

Funding Sources

Authors J.R.S, G.M., and A.W.C. received funding from: The Leverhulme Trust (grant RPG-2014-343); EPSRC (grant EP/P51133X/1); and BBSRC (grant BB/N016734/1),

Notes

All data relating to the work outlined in the article can be found here:

http://dx.doi.org/10.5525/gla.researchdata.608

ACKNOWLEDGMENT

This work was supported by The Leverhulme Trust (grant RPG-2014-343), EPSRC (grant EP/P51133X/1), and BBSRC (grant BB/N016734/1). The authors also wish to thank all the staff working in the James Watt Nanofabrication Centre for their support.

ABBREVIATIONS

AFM, atomic force microscopy; BSA, bovine serum albumin; CPR, change in position response; DI, deionized (water); DNA, deoxyribonucleic acid; FoM, figure of merit; FWHM, full-width half-maximum; HSQ, hydrogen silsesquioxane; LSPR, localized surface plasmon resonance; MES, 2-(N-morpholino)ethanesulfonic acid; MUA, 11-mercaptoundecanoic acid; NIR, near-infrared light; PBS, phosphate buffer saline; PDMS, polydimethylsiloxane; PMMA, ploy(methyl methacrylate); RI, refractive index; RIU, refractive index unit; SAM, self-assembled monolayer; SEM, scanning-electron microscopy; SPR, surface plasmon resonance; UV, ultra-violet light; VIS, visible light.

REFERENCES

(1) Homola, J. Surface Plasmon Resonance Sensors for Detection of Chemical and Biological Species. *Chem. Rev.* **2008,** *108* (2), 462-493, DOI: 10.1021/cr068107d.

(2) Acimovic, S. S.; Ortega, M. A.; Sanz, V.; Berthelot, J.; Garcia-Cordero, J. L.; Renger, J.; Maerkl, S. J.; Kreuzer, M. P.; Quidant, R. Lspr Chip for Parallel, Rapid, and Sensitive Detection of Cancer Markers in Serum. *Nano Lett.* **2014,** *14* (5), 2636-2641, DOI: 10.1021/nl500574n.

(3) Acimovic, S. S.; Sipova, H.; Emilsson, G.; Dahlin, A. B.; Antosiewicz, T. J.; Kall, M. Superior Lspr Substrates Based on Electromagnetic Decoupling for on-a-Chip High-Throughput Label-Free Biosensing. *Light: Sci. Appl* **2017,** *6*, DOI: 10.1038/lsa.2017.42.

(4) Svedendahl, M.; Chen, S.; Dmitriev, A.; Kall, M. Refractometric Sensing Using Propagating Versus Localized Surface Plasmons: A Direct Comparison. *Nano Lett*. **2009,** *9* (12), 4428-4433, DOI: 10.1021/nl902721z.
(5) Unser, S.; Bruzas, I.; He, J.; Sagle, L. Localized Surface Plasmon Resonance Biosensing: Current Challenges and Approaches. *Sensors* **2015,** *15* (7), 15684-15716, DOI: 10.3390/s150715684.
(6) Mayer, K. M.; Hafner, J. H. Localized Surface Plasmon Resonance Sensors. *Chem. Rev*. **2011,** *111* (6), 3828-3857, DOI: 10.1021/cr100313v.
(7) Szunerits, S.; Boukherroub, R. Sensing Using Localised Surface Plasmon Resonance Sensors. *Chem. Commun. (Cambridge)* **2012,** *48* (72), 8999-9010, DOI: 10.1039/c2cc33266c.
(8) Langer, J.; Novikov, S. M.; Liz-Marzan, L. M. Sensing Using Plasmonic Nanostructures and Nanoparticles. *Nanotechnology* **2015,** *26* (32), DOI: 10.1088/0957-4484/26/32/322001.
(9) Sagle, L. B.; Ruvuna, L. K.; Ruemmele, J. A.; Van Duyne, R. P. Advances in Localized Surface Plasmon Resonance Spectroscopy Biosensing. *Nanomedicine* **2011,** *6* (8), 1447-1462, DOI: 10.2217/nnm.11.117.
(10) Fernandez, F.; Garcia-Lopez, O.; Tellechea, E.; Asensio, A. C.; Cornago, I. Lspr Cuvette for Real-Time Biosensing by Using a Common Spectrophotometer. *IEEE Sens. J*. **2016,** *16* (11), 4158-4165, DOI: 10.1109/jsen.2016.2544953.
(11) Sonnichsen, C.; Reinhard, B. M.; Liphardt, J.; Alivisatos, A. P. A Molecular Ruler Based on Plasmon Coupling of Single Gold and Silver Nanoparticles. *Nat. Biotechnol*. **2005,** *23* (6), 741-745, DOI: 10.1038/nbt1100.
(12) Yoo, S. Y.; Kim, D.-K.; Park, T. J.; Kim, E. K.; Tamiya, E.; Lee, S. Y. Detection of the Most Common Corneal Dystrophies Caused by Bigh3 Gene Point Mutations Using a Multispot Gold-Capped Nanoparticle Array Chip. *Anal. Chem*. **2010,** *82* (4), 1349-1357, DOI: 10.1021/ac902410z.
(13) Verdoold, R.; Gill, R.; Ungureanu, F.; Molenaar, R.; Kooyman, R. P. N. Femtomolar DNA Detection by Parallel Colorimetric Darkfield Microscopy of Functionalized Gold Nanoparticles. *Biosens. Bioelectron*. **2011,** *27* (1), 77-81, DOI: 10.1016/j.bios.2011.06.019.
(14) Wadell, C.; Langhammer, C. Drift-Corrected Nanoplasmonic Hydrogen Sensing by Polarization. *Nanoscale* **2015,** *7* (25), 10963-10969, DOI: 10.1039/c5nr01818h.
(15) Liu, Y.; Liu, Q.; Chen, S.; Cheng, F.; Wang, H.; Peng, W. Surface Plasmon Resonance Biosensor Based on Smart Phone Platforms. *Sci. Rep*. **2015,** *5*, DOI: 10.1038/srep12864.
(16) Nenninger, G. G.; Clendenning, J. B.; Furlong, C. E.; Yee, S. S. Reference-Compensated Biosensing Using a Dual-Channel Surface Plasmon Resonance Sensor System Based on a Planar Lightpipe Configuration. *Sens. Actuators, B* **1998,** *51* (1-3), 38-45, DOI: 10.1016/s0925-4005(98)00218-4.
(17) Lu, H. B.; Homola, J.; Campbell, C. T.; Nenninger, G. G.; Yee, S. S.; Ratner, B. D. Protein Contact Printing for a Surface Plasmon Resonance Biosensor with on-Chip Referencing. *Sens. Actuators, B* **2001,** *74* (1-3), 91-99, DOI: 10.1016/s0925-4005(00)00716-4.
(18) Boozer, C.; Yu, Q. M.; Chen, S. F.; Lee, C. Y.; Homola, J.; Yee, S. S.; Jiang, S. Y. Surface Functionalization for Self-Referencing Surface Plasmon Resonance (Spr) Biosensors by Multi-Step Self-Assembly. *Sens. Actuators, B* **2003,** *90* (1-3), 22-30, DOI: 10.1016/s0925-4005(03)00017-0.

(19) Wu, S. Y.; Ho, H. P.; Law, W. C.; Lin, C. L.; Kong, S. K. Highly Sensitive Differential Phase-Sensitive Surface Plasmon Resonance Biosensor Based on the Mach-Zehnder Configuration. *Opt. Lett.* **2004,** *29* (20), 2378-2380, DOI: 10.1364/ol.29.002378.
(20) Levy, R.; Ruschin, S. Design of a Single-Channel Modal Interferometer Waveguide Sensor. *IEEE Sens. J.* **2009,** *9* (1-2), 146-153, DOI: 10.1109/jsen.2008.2011075.
(21) Kashif, M.; Bakar, A. A. A.; Hashim, F. H. Analysing Surface Plasmon Resonance Phase Sensor Based on Mach-Zehnder Interferometer Technique Using Glycerin. *Opt. Commun.* **2016,** *380*, 419-424, DOI: 10.1016/j.optcom.2016.06.033.
(22) Pacholski, C.; Sartor, M.; Sailor, M. J.; Cunin, F.; Miskelly, G. M. Biosensing Using Porous Silicon Double-Layer Interferometers: Reflective Interferometric Fourier Transform Spectroscopy. *J. Am. Chem. Soc.* **2005,** *127* (33), 11636-11645, DOI: 10.1021/ja0511671.
(23) Pacholski, C.; Yu, C.; Miskelly, G. M.; Godin, D.; Sailor, M. J. Reflective Interferometric Fourier Transform Spectroscopy: A Self-Compensating Label-Free Immunosensor Using Double-Layers of Porous Sio2. *J. Am. Chem. Soc.* **2006,** *128* (13), 4250-4252, DOI: 10.1021/ja056702b.
(24) Hao, N.; Zhang, Y.; Zhong, H.; Zhou, Z.; Hua, R.; Qian, J.; Liu, Q.; Li, H.; Wang, K. Design of a Dual Channel Self-Reference Photoelectrochemical Biosensor. *Anal. Chem.* **2017,** *89* (19), 10133-10136, DOI: 10.1021/acs.analchem.7b03132.
(25) Wang, X.; Chang, T.-W.; Lin, G.; Gartia, M. R.; Liu, G. L. Self-Referenced Smartphone-Based Nanoplasmonic Imaging Platform for Colorimetric Biochemical Sensing. *Anal. Chem.* **2017,** *89* (1), 611-615, DOI: 10.1021/acs.analchem.6b02484.
(26) Wersall, M.; Verre, R.; Svedendahl, M.; Johansson, P.; Kall, M.; Shegai, T. Directional Nanoplasmonic Antennas for Self-Referenced Refractometric Molecular Analysis. *J. Phys. Chem. C* **2014,** *118* (36), 21075-21080, DOI: 10.1021/jp5064929.
(27) Rivero, P. J.; Ibanez, E.; Goicoechea, J.; Urrutia, A.; Matias, I. R.; Arregui, F. J. A Self-Referenced Optical Colorimetric Sensor Based on Silver and Gold Nanoparticles for Quantitative Determination of Hydrogen Peroxide. *Sens. Actuators, B* **2017,** *251*, 624-631, DOI: 10.1016/j.snb.2017.05.110.
(28) ChemBuddy Refractive Indices of Sucrose Solutions at 20 °C, 589.29 Nm. http://www.refractometer.pl/refraction-datasheet-sucrose (accessed 2017/08/01).
(29) Jain, P. K.; El-Sayed, M. A. Plasmonic Coupling in Noble Metal Nanostructures. *Chem. Phys. Lett.* **2010,** *487* (4-6), 153-164, DOI: 10.1016/j.cplett.2010.01.062.
(30) Sherry, L. J.; Chang, S. H.; Schatz, G. C.; Van Duyne, R. P.; Wiley, B. J.; Xia, Y. N. Localized Surface Plasmon Resonance Spectroscopy of Single Silver Nanocubes. *Nano Lett.* **2005,** *5* (10), 2034-2038, DOI: 10.1021/nl0515753.
(31) Galush, W. J.; Shelby, S. A.; Mulvihill, M. J.; Tao, A.; Yang, P.; Groves, J. T. A Nanocube Plasmonic Sensor for Molecular Binding on Membrane Surfaces. *Nano Lett.* **2009,** *9* (5), 2077-2082, DOI: 10.1021/nl900513k.
(32) Little, T. A. Method Validation Essentials, Limit of Blank, Limit of Detection, and Limit of Quantitation. *BioPharm Int.* **2015,** *28* (4), 48-51.
(33) Lopez-Munoz, G. A.; Estevez, M. C.; Cristina Pelaez-Gutierrez, E.; Homs-Corbera, A.; Carmen Garcia-Hernandez, M.; Ignacio Imbaud, J.; Lechuga, L. M. A Label-Free Nanostructured Plasmonic Biosensor Based on Blu-Ray Discs with Integrated Microfluidics for Sensitive Biodetection. *Biosens. Bioelectron.* **2017,** *96*, 260-267, DOI: 10.1016/j.bios.2017.05.020.

(34) Haes, A. J.; Van Duyne, R. P. A Nanoscale Optical Blosensor: Sensitivity and Selectivity of an Approach Based on the Localized Surface Plasmon Resonance Spectroscopy of Triangular Silver Nanoparticles. *J. Am. Chem. Soc.* **2002,** *124* (35), 10596-10604, DOI: 10.1021/ja020393x.

TABLE OF CONTENTS FIGURE